

Atmospheric dynamics on terrestrial planets with eccentric orbits

ILAI GUENDELMAN¹ AND YOHAI KASPI¹

¹*Department of Earth and Planetary Sciences, Weizmann Institute of Science
234 Herzl st., 76100
Rehovot, Israel*

Submitted to APJ

ABSTRACT

The insolation a planet receives from its parent star is the main engine of the climate and depends on the planet's orbital configuration. Planets with non-zero obliquity and eccentricity will experience seasonal insolation variations. As a result, the climate will have a seasonal cycle, with its strength depending on the orbital configuration, and atmospheric characteristics. In this study, using an idealized general circulation model, we examine the climate response to changes in eccentricity for both zero and non-zero obliquity planets. In the zero obliquity case, a comparison between the seasonal response to changes in eccentricity and perpetual changes in the solar constant shows that the seasonal response strongly depends on the orbital period and radiative timescale. More specifically, using a simple energy balance model, we show the importance of the latitudinal structure of the radiative timescale in the climate response. We also show that the response strongly depends on the atmospheric moisture content. The combination of an eccentric orbit with non-zero obliquity is complex, as the insolation also depends on the perihelion position. Although the detailed response of the climate to variations in eccentricity, obliquity, and perihelion is involved, the circulation is constrained mainly by the thermal Rossby number and latitude of maximum temperature. Finally, we discuss the importance of different planetary parameters that affect the climate response to orbital configuration variations.

Keywords: atmospheric dynamics — terrestrial planets — eccentricity

1. INTRODUCTION

The climate on a planetary body is sensitive to the planet's characteristics (e.g., [Kaspi & Showman 2015](#); [Komacek & Abbot 2019](#)). In particular, the planet's orbital configuration has significant importance for the climate system, as it dictates the incoming solar radiation. More specifically, the orbital configuration, namely, the obliquity (γ) eccentricity (ε) and perihelion (Π) dictate the insolation seasonal cycle (Fig. 1 depicts a schematics plot of the orbit and the orbital parameters). In addition to the reasonable assumption that a wide set of orbital configurations exist across the universe, the orbital configuration of the different planets changes with a Milankovitch-like cycle ([Spiegel et al. 2010](#)). This

poses the question of how the atmospheric dynamics depends on the orbital configuration.

As eccentricity is a measurable quantity for some of the confirmed exoplanets, one can look at the measured eccentricity distribution, which demonstrates that it spans all eccentricity values (Fig. 2). Focusing on low-mass planets, i.e., planets with mass lower than 10 times the mass of Earth (more relevant for this study), they do not span the entire range of eccentricities, with Kepler-68c having the largest eccentricity value ($\varepsilon = 0.42$, [Gilliland et al. 2013](#)). On one hand, small mass planets may be prone to have small eccentricities ([Howard 2013](#)); on the other hand, it seems that most of the observed low mass planets are in a close-in orbit (Fig. 2), and that with future observations more eccentric low-mass planets will be discovered. Nonetheless, current observations suggest that eccentricity varies within a significant range, motivating the question of how atmospheric dynamics depend on eccentricity.

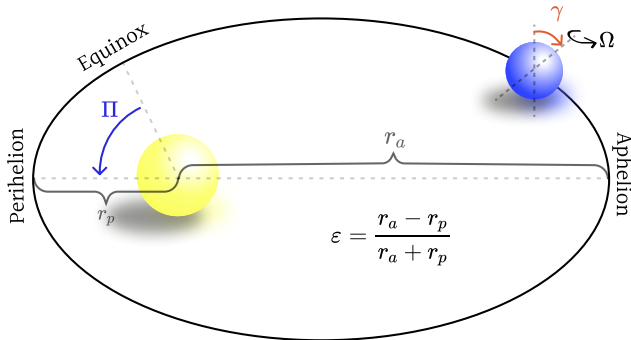


Figure 1. Schematic plot of a planet’s orbit and the relevant parameters, obliquity (γ), eccentricity (ϵ), and perihelion (Π). r_p and r_a are the distances from the star at perihelion and aphelion, respectively, and Ω is the rotation rate.

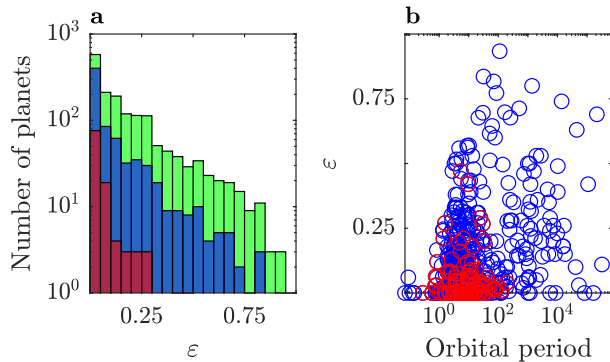


Figure 2. a) Histogram of eccentricity values of the confirmed exoplanets, data taken from the exoplanets.eu catalog. Green represents all planets with measured eccentricity, blue is for all planets with observed mass and red is for all planets with observed mass less than 10 times the mass of Earth. b) Scatter plot of all planets with measured mass, eccentricity and orbital period (in days), blue is for all planets with measured orbital period and eccentricity, and red is for planets with mass less than 10 times the mass of Earth.

Each of the mentioned parameters (γ , ϵ and Π), adds a seasonal cycle of a different nature to the insolation; non-zero obliquity introduces seasonal variations in the latitudinal insolation structure (Fig. 3d-f). The eccentricity seasonal cycle is effectively a seasonal cycle of the solar constant (Fig. 3a-c). The perihelion position becomes important in planets with non-zero obliquity and eccentricity, where the phase between the closest approach (perihelion, higher solar constant) and equinox becomes relevant (see Fig. 3g-i, a more detailed discussion about this point is given in section 4).

The atmospheric response to the seasonally varying insolation will depend on different planetary and at-

mospheric characteristics, specifically, the orbital period and the atmospheric radiative timescale. Longer orbital periods will give the atmosphere more time to adjust to the insolation seasonal cycle, resulting in a stronger seasonal cycle. Longer radiative timescale translates to a weaker seasonal cycle as the atmosphere needs more time to adjust to changes in the radiation (Guendelman & Kaspi 2019).

The effect of eccentricity will vary depending on the orbital configuration of the planet. It is useful to distinguish between three configurations. The first, a tidally locked configuration; in this case, in addition to the variations in the solar constant during the orbital period, on eccentric tidally locked planets, the rotation rate is pseudo-synchronized, such that the rotation rate is synchronized at perihelion, and varies during the orbital period depending on the orbital eccentricity (Hut 1981). Numerous studies were done regarding the effect of eccentricity on the habitability and atmospheric dynamics of tidally locked planets (e.g., Lewis et al. 2010; Kataria et al. 2013; Wang et al. 2014; Lewis et al. 2014; Bolmont et al. 2016). Among them, Kataria et al. (2013) studied the atmospheric dynamics of a tidally locked planet on eccentricity, considering pseudo-synchronization. They showed that over a large range of eccentricities, the circulation characteristics stay similar to a circular tidally locked orbit, and the seasonal changes are mostly quantitative in nature. More recently, Lewis et al. (2017) have studied the extreme case of HD 80606b ($\epsilon = 0.93$); at this extreme case, when considering pseudo-synchronization, the circulation shifts during the orbital period, from a tidally locked climate to a more diurnal mean, zonally symmetric one.

The second and third configurations are for planets where the diurnal mean insolation is the dominant forcing, similar to Earth’s case. The difference between the two is the obliquity, where for one, the obliquity is zero, and for the other, the obliquity is non-zero. For both these cases, previous studies have focused mainly on the question of how eccentricity affects the planetary habitability, and the transition to a snowball state (Williams & Pollard 2002; Dressing et al. 2010; Spiegel et al. 2010; Linsenmeier et al. 2015; Mndez & Rivera-Valentn 2017). The methods used in these studies range from energy balance models (EBM, e.g., Dressing et al. 2010), simple hydrodynamical models (e.g., Adams et al. 2019; Ohno & Zhang 2019) and comprehensive general circulation model (GCM, e.g., Williams & Pollard 2002; Way & Georgarakos 2017). Ohno & Zhang (2019), using a simple 1.5 layer model, studied the climate response to different orbital forcing and radiative timescale, showing that depending on the specific orbital configuration

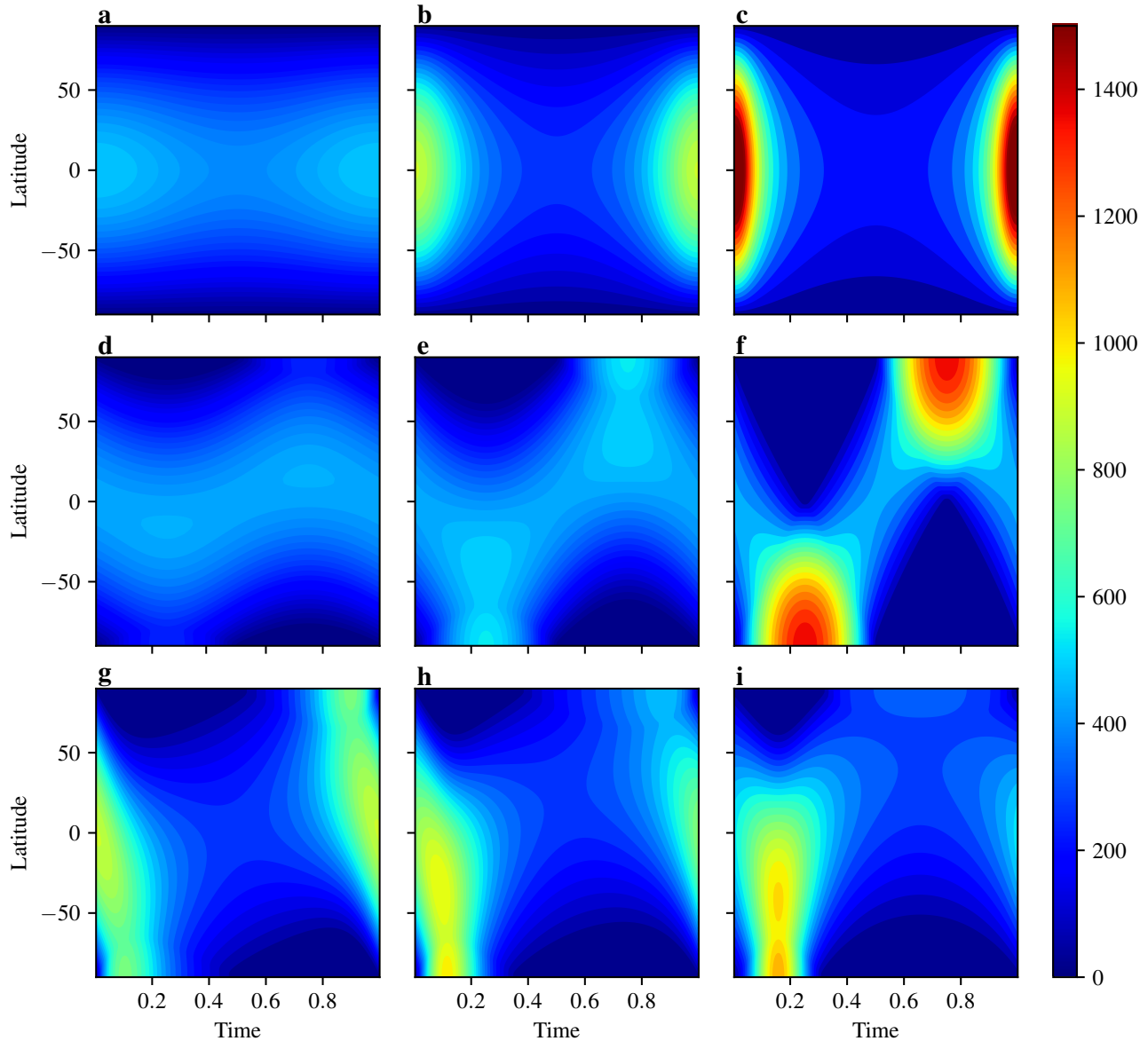


Figure 3. Insolation for different values of eccentricity, obliquity and perihelion. Panels a-c are zero obliquity cases with $\epsilon = 0.05, 0.3, 0.5$ from left to right, respectively. Panels d-f are zero eccentricity cases with $\gamma = 10^\circ, 23^\circ, 90^\circ$ from left to right, respectively, with perihelion at 0° . Panels g-i are for $\epsilon = 0.3$ and $\gamma = 23^\circ$ with perihelion $0^\circ, 45^\circ$ and 90° from left to right, respectively.

and radiative timescale, the climate changes from annual mean climate to seasonally varying climate. In addition, they showed that in some configurations during the seasonal cycle, there is a transition from a climate that is controlled by the diurnal mean to a climate controlled by the diurnal cycle.

In this study, we use an idealized GCM, to systematically study the effect of eccentricity on the climate. For simplicity, we focus on the diurnal mean forcing and explore eccentricity values up to 0.5. The simplest configuration of a seasonal cycle due to eccentricity is plan-

ets with zero obliquity. As the seasonal cycle on planets in an eccentric orbit with zero obliquity is equivalent to seasonal variation in the solar constant, we start by considering the effect of changing the solar constant on a perpetual equinox case in section 2. We show that the climate response differs between dry and moist atmospheres, a result of the nonlinear response of moisture to changes in temperature. The perpetual equinox case acts as a baseline for the study of the seasonal cycle on planets in an eccentric orbit with zero eccentricity in section 3. In section 4, we present the complexity that

arises when combining eccentricity and obliquity, giving constraints on the circulation response and discussing the important parameters in this problem. Finally, we conclude our results in section 5.

2. PERPETUAL SOLAR CONSTANT VARIATIONS

Studies of the eccentricity effect on planets with zero obliquity are few and focus mainly on the temperature response and less on the dynamics (e.g., Dressing et al. 2010; Ohno & Zhang 2019). Kane & Torres (2017) compared the effect of eccentricity and obliquity on the insolation, showing that even for low eccentricity values, the effect of eccentricity is significant. Motivated by that, and for the sake of completeness, we start by first examining the more simple case of zero obliquity planets before diving into the more complex cases.

An idealized general circulation model with a seasonal cycle (Guendelman & Kaspi 2019) is used in this study. This model has a simplified moisture representation (Frierson et al. 2006). For simplicity, the optical depth is taken to be constant in latitude, meaning we neglect water-vapor feedback. Although using a more complex GCM, which includes water vapor feedback, clouds, and sea-ice, might affect the results, the idealized configuration is a good starting point to study the climate sensitivity to eccentricity.

The insolation variations during an eccentric orbit of a zero obliquity planet are equivalent to changes in the solar constant (S_0) during the orbit. For this reason, before focusing on the eccentricity seasonal cycle, it is beneficial to study the response of the perpetual case to changes in the solar constant. Most previous studies of the climate dependence on the solar constant were done with the purpose of determining planetary habitability (e.g., Kopparapu et al. 2013; Wolf et al. 2017). In addition, studies that do focus on the atmospheric dynamics response to the solar constant variations were done as part of large parameter swipes, discussing only briefly the solar constant effect (e.g., Kaspi & Showman 2015; Komacek & Abbot 2019). In addition to the trivial warming with S_0 , Kaspi & Showman (2015) found that the normalized equator-to-pole temperature difference

$$\Delta_T = \frac{\max(T_s) - \min(T_s)}{\text{mean}(T_s)}, \quad (1)$$

where T_s is the surface temperature, changes in a non-monotonic form with S_0 , where for small S_0 , Δ_T increases with S_0 and for high S_0 , Δ_T decreases with S_0 (Fig. 4a). Kaspi & Showman (2015) attributed the non-monotonic behavior of Δ_T with S_0 to the non-linearity of moisture with temperature. This non-linearity results with more efficient equator-to-pole heat transport as the

climate gets warmer (Fig. 4b). The total heat transport can be described in terms of the moist static energy (MSE), $m = Lq + s$, where L is the latent heat of vaporization, q is the specific humidity, and $s = C_p T + gz$ is the dry static energy, where C_p is the heat capacity of dry air, T is temperature, g is surface gravity, and z is geopotential height. The zonal mean MSE flux, \overline{vm} , where v is the meridional wind and bar denotes zonal mean, can be divided into contributions from the zonal mean and eddies (deviations from the zonal mean, denoted by a prime, for a general field A , $A' = A - \bar{A}$) in the following form

$$\overline{vm} = \overline{v\bar{m}} + \overline{v'm'} = L\overline{vq} + \overline{v\bar{s}} = L\overline{vq} + \overline{v\bar{s}} + \overline{Lv'q'} + \overline{v's'}. \quad (2)$$

Increasing the solar constant results in an increase in the total heat flux, with the main contribution coming from the eddy fluxes (Fig. 5). In particular, the moist contribution becomes more dominant as the solar constant increases in a nonlinear form (Figures 5 and 4b). This non-linearity of the MSE flux explains the non-monotonic behavior of Δ_T with S_0 (Kaspi & Showman 2015). In order to illustrate this, it is convenient to look at the Clausius-Clapeyron equation for the saturation water vapor pressure in the atmosphere

$$e_s(T) = e_0 \exp \left[-\frac{L}{R_v} \left(\frac{1}{T} - \frac{1}{T_0} \right) \right], \quad (3)$$

where R_v is the gas constant for water vapor and e_0 is the saturation vapor pressure at $T_0 = 273.16^\circ\text{K}$. This non-linearity will result in higher e_s at warmer latitudes. Increasing the solar constant will enhance this effect, resulting in an increased moisture meridional gradient; in order to flatten this gradient, the flux will increase, resulting in more heat transported from the equator to the poles.

To verify that the non-monotonic behavior of Δ_T with S_0 is a result of moisture, it is convenient to follow the approach of Frierson et al. (2006), setting e_0 to zero in order to eliminate moisture from the simulations. Indeed in this 'dry' model configuration, Δ_T strictly increases with S_0 (Fig. 4a). In addition, the dry and moist simulations exhibit other significant differences; first, the dry simulations are warmer than the moist ones, since, in the moist simulations, water evaporation acts as an energy sink that does not exist in dry simulations. In addition to the all-around cooling in the moist simulation, the evaporation is stronger at the equatorial regions, cooling the equator more than the poles, resulting in a weaker equator-to-pole temperature difference in the moist simulations (Fig 4a).

The moist and dry simulations also differ in the tropopause height and the lapse rate (Fig. 4d-e). While

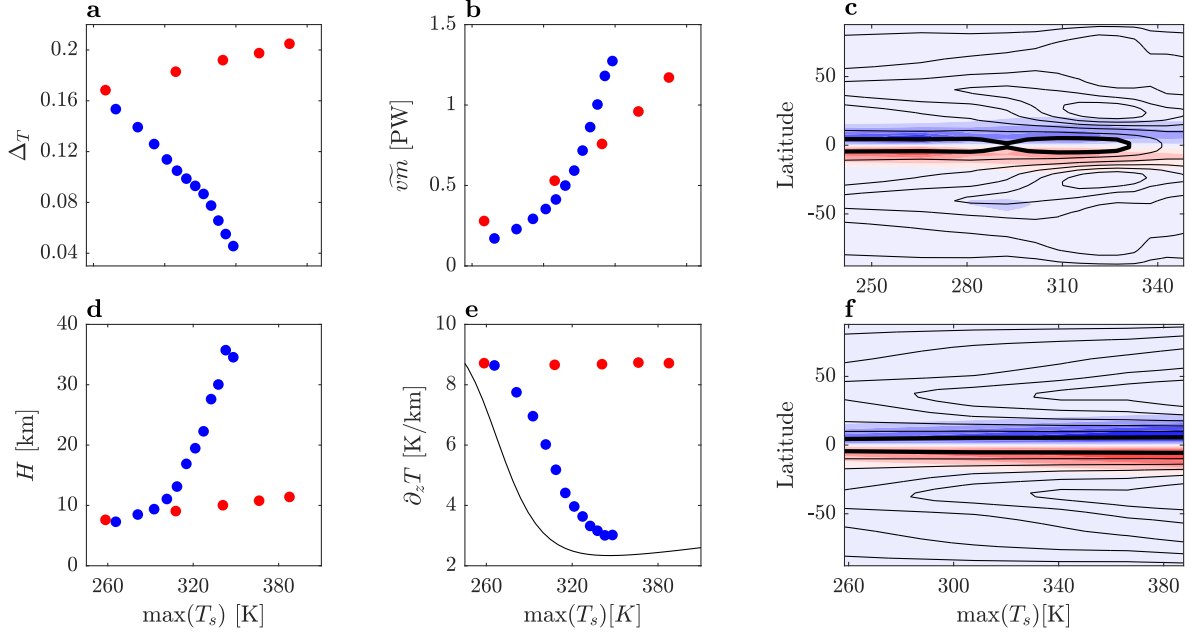


Figure 4. Comparison between moist (blue dots) and dry simulation (red dots) for increasing value of S_0 (corresponds to increasing value of maximum surface temperature ($\max(T_s)$)). Note that for the moist simulations the range of S_0 is $500 - 3500 \text{ Wm}^{-2}$, and for the dry simulations the range of S_0 is $500 - 2500 \text{ Wm}^{-2}$. Panels a, b, d and e are the normalized meridional temperature gradient (Δ_T), Northern Hemisphere mean MSE flux ($\bar{v}m$) tropopause height (H) and tropospheric lapse rate ($\partial_z T$) as a function of $\max(T_s)$, respectively. Panels c and f, respectively, are the moist and dry mean meridional circulation (colors, vertically averaged between 400 and 600 mbar, blue means northward flow in the upper branch of the circulation), and the zonal mean zonal wind (contours, vertically averaged between 100 and 500 mbar), where the bold contour represents the zero zonal mean zonal wind line. Note that the colorscale differs, where in c it is $\pm 1 \times 10^{11} \text{ kg s}^{-1}$ and in f it is $\pm 2 \times 10^{11} \text{ kg s}^{-1}$. The black line in panel e is the saturation moist adiabat at 600 mbar.

the lapse rate in the dry simulations remains constant across the different S_0 values, for the moist case, it decreases with S_0 (Fig. 4e). This difference is a result of the atmosphere relaxing towards a different relevant adiabatic lapse. While the dry adiabat, $\Gamma_d = g/c_p$, is determined by planetary parameters that are independent of S_0 ; in the moist case, the relevant lapse rate is the saturation moist adiabatic lapse rate, that can be written as

$$\Gamma_m = \Gamma_d \frac{1 + \frac{L\mu_s}{R_d T}}{1 + \frac{L^2\mu_s}{C_p R_v T^2}}, \quad (4)$$

where $\mu_s = R_d e_s(T)/R_v p$ is the saturation mixing ratio and R_d is the gas constant of dry air (Andrews 2010). Γ_m represents the lower limit for the lapse rate, where it is lower than the dry adiabat and generally decreases with temperature (black line in Fig. 4e).

The difference in the tropopause height response between the simulations can be explained by using the equation for the tropopause height from Vallis et al. (2015)

$$H = \frac{1}{16\Gamma} \left(CT_{\text{trop}} + \sqrt{C^2 T_{\text{trop}}^2 + 32\Gamma\tau_s H_s T_{\text{trop}}} \right), \quad (5)$$

where Γ is the lapse rate, C is a constant, T_{trop} is the tropopause temperature, τ_s is the optical depth at the surface and H_s is the atmospheric height scale. H is proportional to T_{trop} , which increases with S_0 in both the dry and moist cases. In addition to that, H is inversely proportional to Γ , which decreases only in the moist case. This can explain the difference in the response of H between moist and dry simulations.

These changes in Δ_T , H , and lapse rate, can be used to explain how the atmospheric dynamics changes as a function of S_0 , more specifically, the changes in the zonal mean zonal wind \bar{u} , and in the mean meridional circulation ψ , as a function of S_0 . The mean meridional circulation is described using the mean meridional streamfunction

$$\psi = \frac{2\pi a}{g} \int \bar{v} \cos \phi dp, \quad (6)$$

where a is the planetary radius, ϕ is latitude, and p is pressure. On Earth, the meridional circulation is composed mainly of the tropical thermally driven Hadley cell, where, in the annual mean, air rises at the equator and descends at the subtropics. At the midlatitudes, there is the eddy-driven Ferrel cell, which is

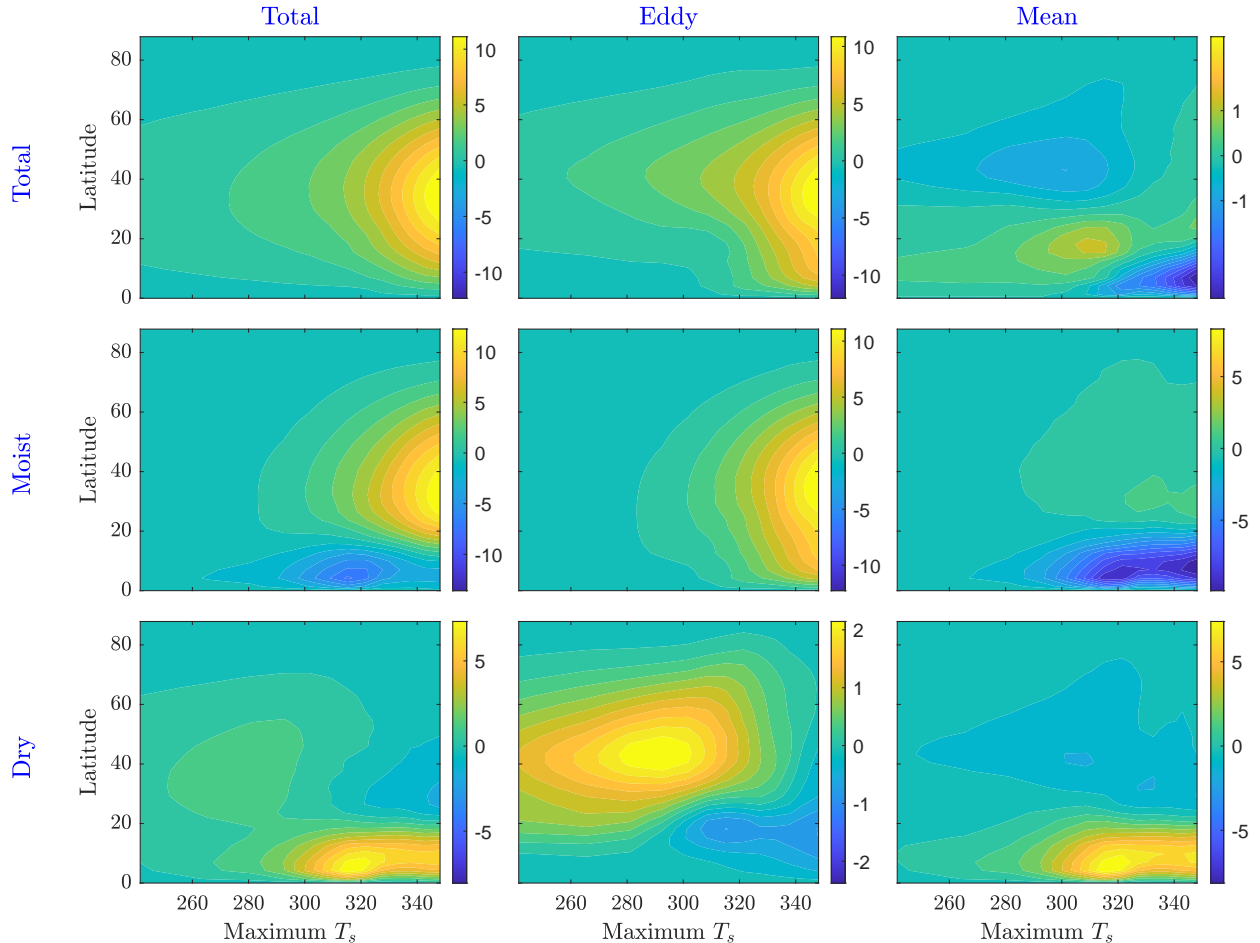


Figure 5. Vertically integrated moist static energy flux and its decomposition (Eq. 2) as a function of maximum surface temperature. Increasing maximum surface temperature corresponds to increasing solar constant ranging from 500 to 3500 Wm^{-2} . Note that each subplot has its own color-scale (PW).

driven by turbulence in the atmosphere (Vallis 2017). In both moist and dry cases, \bar{u} and ψ have relatively small changes with S_0 , with a general increase in the jet strength with S_0 and small changes in the streamfunction (Fig. 4c,f). The streamfunction has a different response between the dry and moist cases, where for the dry case, the circulation increases with S_0 , whereas, for the moist case, it decreases with S_0 . This behavior correlates with the response of Δ_T to S_0 , and in agreement with theoretical arguments from the axisymmetric theory, where the strength of the circulation is proportional to the meridional temperature gradient (Held & Hou 1980). This should be taken with a grain of salt, as according to the Held & Hou (1980) scaling, the strength should increase with higher H ; however, it was shown that the relation between H and the circulation strength

is not as robust as the relation between Δ_T and the circulation strength (Chemke & Kaspi 2017).

For the moist case, simulations with high values of S_0 , exhibit equatorial superrotation (Fig. 4c). A possible reason for the transition to superrotation is the decrease in Δ_T with the solar constant, which was shown to result in superrotation for some cases (Laraia & Schneider 2015; Polichtchouk & Cho 2016). As the equator-to-pole temperature difference decreases, baroclinicity becomes weaker, allowing superrotation to develop from a wave source in the equatorial region (Polichtchouk & Cho 2016). Determining the specific mechanisms responsible for the superrotation transition in the simulations is out of the scope of this study.

3. THE SEASONAL CYCLE ON A PLANET IN AN ECCENTRIC ORBIT WITH ZERO OBLIQUITY

3.1. Temperature response

The insolation seasonal cycle of a planet in an eccentric orbit with zero obliquity can be described as seasonal variations of the solar constant. The atmospheric response to the seasonal cycle insolation is dominated by some ratio of the radiative timescale and the orbital period (Rose et al. 2017; Guendelman & Kaspi 2019). Longer orbital periods give the atmosphere more time to adjust to seasonally varying insolation, resulting in a more significant seasonal climate (Guendelman & Kaspi 2019). The radiative timescale can be written as

$$\tau_{\text{rad}} = \frac{C}{4\sigma T_e^3}, \quad (7)$$

where C is the atmospheric heat capacity, σ is the Stefan-Boltzmann constant and T_e is the equilibrium temperature,

$$T_e = \left(\frac{Q}{\sigma}\right)^{1/4}, \quad (8)$$

where Q is the incoming insolation at the top of the atmosphere. The radiative timescale controls the time that the atmosphere will need to adjust to radiative changes. Substituting Equation 8 into Equation 7 gives $\tau_{\text{rad}} \propto Q^{-3/4}$, meaning, the radiative timescale is inversely proportional to the top of the atmospheric incoming radiation. Alternatively, as the temperature is colder, the atmospheric response to radiative changes is longer.

In planets with zero obliquity, there is hemispherical symmetry, due to this symmetry, it is convenient to quantify the surface temperature seasonal cycle using ΔT and $\max(T_s)$. In this $(\Delta T, \max(T_s))$ space, the seasonal cycle has a shape of an ellipse, this shape changes its characteristics depending on the eccentricity and orbital period values, as shown in Figure 6, where the red circle denotes the first day of the year, and the seasonal cycle goes clockwise. Increasing eccentricity in an Earth-like orbital period (Fig. 6a,d) results in a stronger seasonal cycle, with most of the response occurring in the cooling period in the seasonal cycle. This is a result of the differences between the timescale of the cooling and warming periods during the insolation seasonal cycle; where although the maximum (minimum) insolation increases (decreases) strongly (weakly) with eccentricity, the time period of this strong warming (weak cooling) becomes shorter (longer) with eccentricity (Fig. 3a-c) giving the atmosphere less (more) time to adjust these radiative changes. Compared to that, increasing eccentricity in a short orbital period (1/8 of Earth's), although the seasonal cycle (which is small) increases with eccentricity, its response is more linear

(Fig. 6b,e), mainly because, in this case, the atmosphere has very little time to adjust to the radiative changes. In addition to the seasonal cycle changes, there is general warming with eccentricity; this warming is the response to the annual mean insolation. The annual mean insolation increases with eccentricity (Bolmont et al. 2016), for this reason, if the orbital period is short enough, the climate is forced effectively by the annual mean insolation resulting in a general warming trend, with the ΔT response following the perpetual response (lines in Fig. 6).

The response of changing the orbital period in constant eccentricity (Fig. 6c,f), has qualitative differences. First, increasing the orbital period changes both the cooling and warming period response, a result of the fact that increasing the orbital period gives more time for the atmosphere to adjust in both these periods. The second main response of the seasonal cycle with the orbital period is that the general slope of ΔT with $\max(T_s)$ changes with the orbital period. We can use the following matrices to quantify this result

$$\Delta \max(T_s) = \max(\max(T_s)) - \min(\max(T_s)), \quad (9)$$

$$\Delta[\Delta T] = \max(\Delta T) - \min(\Delta T), \quad (10)$$

$$\alpha = \frac{\Delta T(\max(\max(T_s))) - \Delta T(\min(\max(T_s)))}{\Delta \max(T_s)}, \quad (11)$$

where $\Delta \max(T_s)$ and $\Delta[\Delta T]$ represents the seasonal amplitude of changes in $\max(T_s)$ and ΔT respectively, note that increase in $\Delta \max(T_s)$ is equivalent to increase in the orbital period. α represents the mean slope of ΔT as a function of $\max(T_s)$. Both $\Delta[\Delta T]$ and α are non-monotonic with orbital period, for both dry and moist cases, both increase in short orbital period and decrease in long ones (Fig. 7).

A good starting point to understand the non-monotonic dependence of α and $\Delta[\Delta T]$ on the orbital period is to consider the extremes. The first, a very short orbital period, where we expect a weak seasonal cycle signal, and can be represented as a point (in Fig. 6). The second, an 'infinite orbital period', this case is equivalent to changing the solar constant in a perpetual climate, the seasonal cycle will coincide with the line for the perpetual case (black and red lines in Fig. 6). Using these, it becomes clear why the seasonal cycle in long orbital periods approaches to the perpetual line, and so does the decrease of α and $\Delta[\Delta T]$ at long orbital periods. The remaining question is, what controls the shape of the seasonal cycle in short to moderate orbital periods?

3.1.1. Simple Energy balance model

For long orbital periods, α starts to decrease, as a result of the atmosphere having enough time to respond

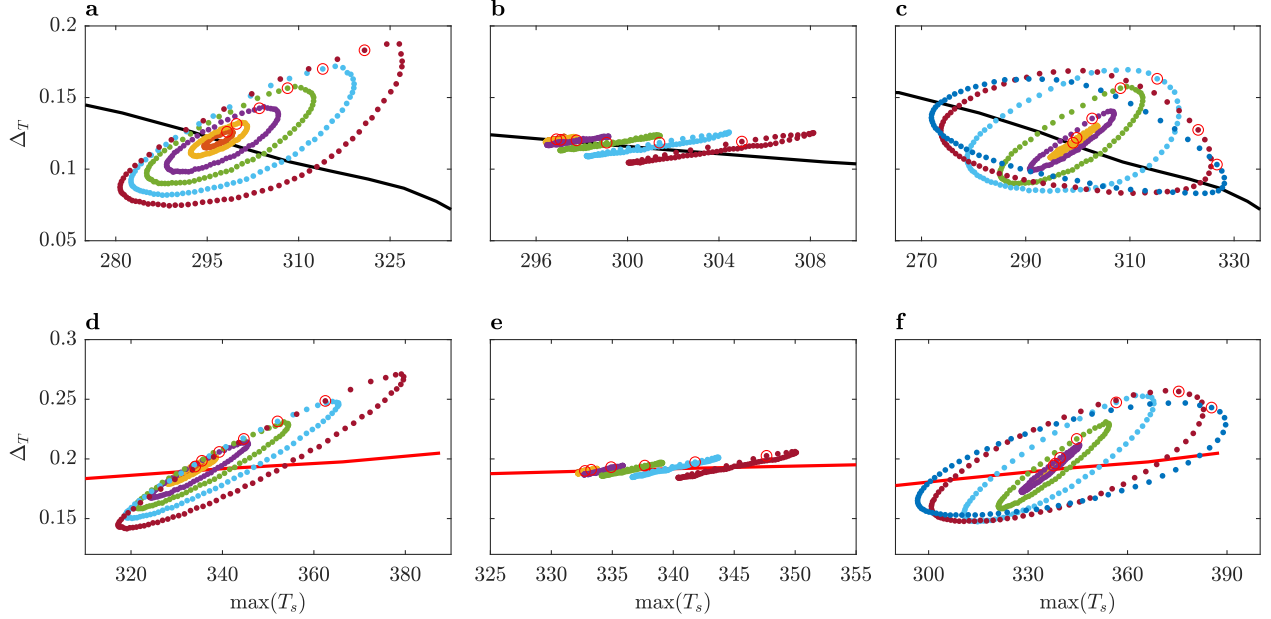


Figure 6. Δ_T as a function of $\max(T_s)$ for different values of eccentricity (0.05 (blue), 0.1 (orange), 0.2 (yellow), 0.3 (purple), 0.4 (green), 0.5 (cyan)), with Earth-like orbital period (a,d) and 1/8 of Earth's orbital period (b,e) and for different orbital period (0.125 (blue), 0.25 (orange), 0.5 (yellow), 1 (purple), 2 (green), 4 (cyan), 6 (bordeaux) times Earth's orbital period) with $\epsilon = 0.3$ (c,f) for moist (first row) and dry (second row) simulations. Red circles represents the first day of the year, also the day with maximum insolation (the seasonal cycle goes clockwise). Black and red lines are the line from the perpetual equinox simulations (Fig. 4a), for moist and dry, respectively.

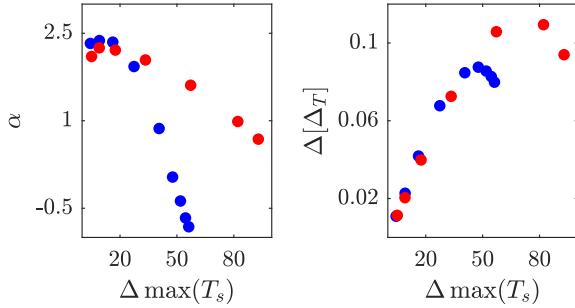


Figure 7. α (left panel), the mean slope of Δ_T with respect to $\max(T_s)$ from Figure 6c,f, and $\Delta[\Delta_T]$ (right panel) the seasonal amplitude of Δ_T as a function of $\Delta(\max(T_s))$, where increase in $\Delta(\max(T_s))$ is equivalent to increase in orbital period, for moist (blue) and dry (red) cases.

to the radiative changes, and the dynamics to kick in to change the temperature structure. Given this, we can assume that in short orbital periods, the dynamics do not have enough time to alter the seasonal cycle temperature structure significantly, and the main process is a radiative one. Based on this argument, consider a simple dry, non-diffusive energy balance model,

$$C \frac{dT}{dt} = Q - \sigma T^4, \quad (12)$$

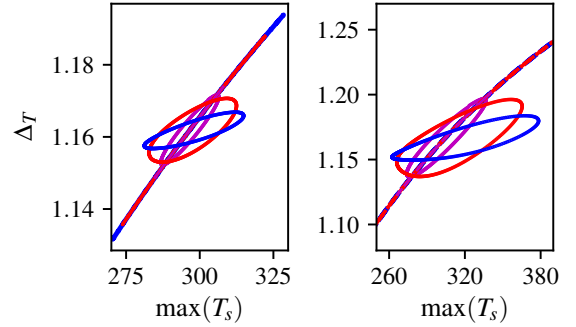


Figure 8. Solution of the simple EBM (Eq. 18) for $\epsilon = 0.1$ (left panel) and 0.3 (right panel) with different values of orbital period (1/8 (purple), 1 (red), 4 (blue)). The lines are solutions with τ_{rad} taken to be constant with latitude, with value of a 30 days, the ellipses are solutions for a latitude dependent τ_{rad} given by Equation 7.

where C is the heat capacity, and Q is the insolation, and both Q and T are a function of time and latitude. To simplify this even further, we can assume that the annual mean is relaxed to the annual mean forcing, this assumption can be justified from Figure 6, where the center of each ellipse falls on or is close to, the perpetual equinox line, suggesting that the annual mean is relaxed to the relevant perpetual equinox scenario. Us-

ing this assumption, the temperature and insolation can be decomposed into

$$T = \bar{T} + T', \quad (13)$$

$$Q = \bar{Q} + Q', \quad (14)$$

where

$$\bar{T} = \left(\frac{\bar{Q}}{\sigma} \right)^{1/4}. \quad (15)$$

Here, the bar and prime notations are the mean and deviations from the mean with respect to time. Assuming that $T' \ll \bar{T}$, we can linearize Equation 12 giving

$$C \frac{dT'}{dt} = Q' - 4\sigma \bar{T}^3 T'. \quad (16)$$

Equation 16 is a linear ordinary differential equation with the general solution

$$T' = \left[\int \frac{Q'}{C} \exp\left(\frac{t}{\tau_{\text{rad}}}\right) dt + T_0 \right] \exp\left(-\frac{t}{\tau_{\text{rad}}}\right), \quad (17)$$

where τ_{rad} is the radiative timescale (as in Eq. 7, substituting T_e with \bar{T}), and T_0 is the initial condition¹. In order to illustrate the role of the orbital period, we can write $t \rightarrow \omega t'$, where ω is the orbital period; using this notation we can write the temperature solution

$$T = \left(\frac{\bar{Q}}{\sigma} \right)^{1/4} + \left[\int \frac{\omega Q'}{C} \exp\left(\frac{\omega}{\tau_{\text{rad}}} t'\right) dt' + T_0 \right] \exp\left(-\frac{\omega}{\tau_{\text{rad}}} t'\right). \quad (18)$$

The nature of the solution strongly depends on the latitudinal structure of τ_{rad} . If τ_{rad} is taken to be the same at all latitudes, the solution is simply a straight line, that becomes longer with the orbital period (Fig. 8). However, taking τ_{rad} with a latitudinal structure (as in Equation 7, with \bar{T}), the temperature solution becomes qualitatively similar to the GCM solution. This result suggests that at least, for the short and moderate orbital periods where ω/τ_{rad} is small enough, the eccentricity seasonal cycle can be explained using these radiation balance arguments. Note that this statement is true only for the seasonal cycle response, that is considered to be a perturbation around the mean state, where the mean state is strongly affected by dynamics and other processes. Once ω/τ_{rad} is large enough, the atmosphere has a longer time to respond to the radiative changes, and other dynamical and nonlinear radiative

effects come into play. Additionally, the simple solution (Eq. 18) dependence on the latitudinal structure of τ_{rad} , underlines the importance of the latitudinal structure of the radiative timescale for the response of the atmosphere to the eccentricity seasonal cycle.

3.2. Circulation response

Meridional temperature gradients will affect the atmospheric general circulation. The balance between the meridional temperature gradients and the circulation can be illustrated from thermal wind balance

$$f \frac{\partial u}{\partial p} = \frac{R_d}{p} \frac{1}{a} \left(\frac{\partial T}{\partial \phi} \right)_p, \quad (19)$$

where $f = 2\Omega \sin \phi$ is the Coriolis parameter, with Ω the rotation rate. The subscript p in the last term of Equation 19, denotes that the derivative is taken over isobaric surfaces. The thermal wind balance is the first order balance for an atmosphere in hydrostatic balance on fast rotating planets (Vallis 2017; Galanti et al. 2017). Equation 19 relates the meridional temperature structure with the vertical wind structure, where steeper meridional temperature gradients are balanced by stronger vertical zonal wind shear. In addition to the effect on the zonal winds, the mean meridional circulation is also strongly affected by the meridional temperature gradients, where the Hadley circulation becomes stronger and wider as the meridional temperature gradient increases (Held & Hou 1980).

Both the meridional streamfunction and the zonal wind exhibit a seasonal cycle that is more pronounced in the moist case (Fig. 9), consistent with the perpetual case where the dynamics had a more complex dependence on S_0 (Fig. 4). However, in contrast to the perpetual moist case, where, for example, warmer climate resulted in a weaker circulation, this is not the case for the seasonal cycle, a result of the different dependence of Δ_T on $\max(T_s)$. Also, the only case where equatorial superrotation persist for the seasonal cycle, if for $\varepsilon = 0.5$ (Fig. 9c), however, it is correlated with high Δ_T , unlike the perpetual case, suggesting that a different mechanism is responsible for the transition to superrotation in the seasonal cycle case.

In rotating atmospheres, two general processes can accelerate a westerly (prograde) jet stream, both involve a source of angular momentum for the prograde flow. The first mechanism relates to the poleward transfer of air from the warm tropic to higher latitudes (e.g., the Hadley circulation). If, in this process, the poleward traveling air conserves its angular momentum, starting with a zero zonal mean zonal wind at the equator, the

¹ T_0 is given by calculating T' with a random value for T_0 for one year and using the last step from this calculation as the initial condition for the solution showed in Figure 8.

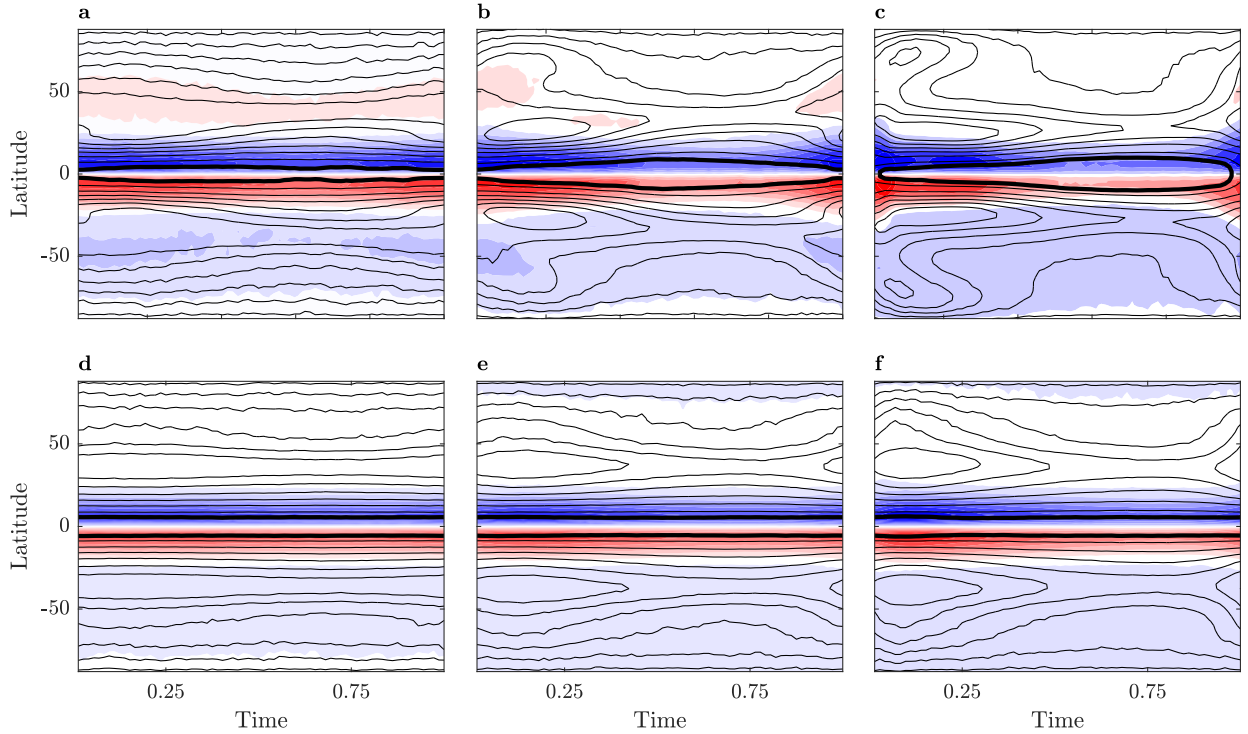


Figure 9. Comparison of moist (top row) and dry (bottom row) seasonal cycle of the meridional circulation averaged vertically between 400 – 600 hPa (shading, blue means northward flow in the upper branch of the circulation) and zonal mean zonal wind (contours) for eccentricities: 0.1 (a,d) 0.3 (b,e) 0.5 (c,f).

angular momentum conserving wind (Vallis 2017) is

$$u_m = \Omega a \frac{\sin^2 \phi}{\cos \phi}. \quad (20)$$

This process will result in a prograde jet at the edge of the Hadley circulation. This type of jet is called a thermally driven jet, on Earth, also the subtropical jet. Note that this is an ideal form to depict this process, and on reality, turbulent and other processes that are neglected in this ideal scheme can be relevant (Levine & Schneider 2015).

The second process that can contribute to the acceleration of prograde jets relates to wave braking in the atmosphere. At the midlatitudes, where the temperature gradients are concentrated, baroclinic² instability develops, creating disturbances at this region of the atmosphere. It can be shown, using potential vorticity (PV) and angular momentum conservation arguments, that disturbances in this region will produce momentum convergence into the disturbance latitudes, resulting in

² Baroclinicity is the measure of the misalignment of density and pressure surfaces, when these surfaces align the fluid is called barotropic.

a prograde jet (Vallis 2017). This type of jet is called an eddy driven jet.

On Earth, these two processes occur in proximity to each other, resulting mainly in a merged state jet, however the jet characteristics changes during the seasonal cycle (Lachmy & Harnik 2014; Vallis 2017; Yuval & Kaspi 2018). Looking at other planets, mainly the gas giants, Saturn and Jupiter, for example, have multiple jets in each hemisphere (Ingersoll 1990). Generally, the number of jets in each hemisphere for a given planetary atmosphere relates to the typical eddy and inverse energy cascade length scale (Rhines 1975, 1979; Chemke & Kaspi 2015a,b). More specifically, the inverse energy cascade scale, i.e., the Rhines scale, L_R is defined to be

$$L_R = \left(\frac{2U}{\beta} \right)^{1/2}, \quad (21)$$

where U is a measure for the zonal wind (the root mean square velocity, often taken as the square of the eddy velocity (Rhines 1975)) and $\beta = 2\Omega \cos \phi/a$. An estimation for the number of jets is given by (Wang et al. 2018)

$$N_j \approx \frac{a}{4L_R}. \quad (22)$$

Wang et al. (2018) and Lee (2005) used different forms to estimate L_R finding that $N_j \propto (\Delta\theta)^{-1/2}$, where $\Delta\theta$ is the equator to pole potential temperature³ difference. (Wang et al. 2018) also tested other estimation for L_R showing it gives a similar result.

As the circulation seasonal cycle response seems to be relatively weak (Fig. 9), it is useful to look at the extreme cases. Following the qualitatively different response of the temperature to changes in eccentricity and orbital period, we compare the circulation response between two simulations, the first is a $\varepsilon = 0.5$ and $\omega = 1$ simulation (hereafter referred as high eccentricity simulation), and the second is a $\varepsilon = 0.3$ and $\omega = 4$ simulation (hereafter referred as long orbital period simulation).

The mean meridional circulation gets stronger as Δ_T becomes stronger for both cases (Fig. 10a,d), this relation can be explained using axisymmetric argument (as mentioned earlier in this manuscript Held & Hou 1980). The height of the circulation becomes higher with higher surface temperature (black contours in Fig. 10b,c,e,f top panels), which is a similar response to the tropopause height in the perpetual case (Fig 4d). Note that qualitative differences in the temperature response result in a qualitative difference in the circulation structure. More specifically, in the high eccentricity simulation, a high surface temperature comes together with a large Δ_T (Fig. 6a), resulting in higher and stronger circulation at high Δ_T (Fig. 10b-c). However, in the long orbital period simulation, a large Δ_T goes with a relatively low surface temperature (Fig. 6c), resulting in a more complex response, where the higher circulation is weaker (Fig. 10e-f).

The zonal mean zonal wind, \bar{u} , also changes characteristics during the seasonal cycle. As mentioned, there are two types of jets, the first, the thermally driven jet, associated with the Hadley circulation and the eddy-driven jet, where on Earth, they are generally co-located. There are several forms to distinguish between the two, first, the thermally driven jet will be located at the edge of the Hadley circulation, whereas the eddy-driven one will be associated with eddy momentum flux convergence. The second is their vertical structure, where the thermally driven jet has a more baroclinic structure, and the eddy-driven jet has more barotropic structure (Vallis 2017).

During the seasonal cycle of both simulations, high eccentricity, and long orbital period, there is a transition from one to two jets (Fig. 10). Following the $(\Delta\theta)^{-1/2}$

scaling, using $\Delta_T^{-1/2}$ as a proxy for it, $\Delta_T^{-1/2}$ shows a good correlation with the number of eddy-driven jets. For both cases, in minimum values of $\Delta_T^{-1/2}$, there is only one eddy-driven jet (Fig. 10b,e); however, in the high eccentricity case, the eddy driven and thermally driven jets are two separated jets (Fig. 10b). In contrast, in the long orbital period case, there is only one merged jet (Fig. 10e). Around maximum values of $\Delta_T^{-1/2}$, in both simulations, there are two eddy driven jets, one merged with the thermally driven jet and the other (relatively weak) at higher latitudes (Fig. 10c,f). Another difference between the two simulations is that for the high eccentricity there is a short period with equatorial superrotation (Fig. 10a), a thing that does not happen in the long orbital period simulation. This superrotation happens when $\Delta_T^{-1/2}$ reaches its minimum values, i.e., high Δ_T values. A manifestation of this superrotation can be seen in Figure 10b, where there is weak eddy momentum flux convergence at the equator. Another distinctive feature, in this case, is that the midlatitude eddy momentum flux convergence is more poleward than all other cases (Fig. 10). This poleward shift of the eddy momentum flux convergence may suggest that the Rossby wave that is responsible for the acceleration of this jet, transports momentum from the subtropics, instead of the tropics, allowing momentum to converge at the equator. This is similar to the mechanism suggested by Mitchell & Vallis (2010) for high and intermediate thermal Rossby numbers,

$$R_o = \frac{2gH\Delta_T}{\Omega^2 a^2}, \quad (23)$$

that can be relevant to this case as Δ_T is high.

4. THE SEASONAL CYCLE ON A PLANET IN AN ECCENTRIC ORBIT WITH NON-ZERO OBLIQUITY

4.1. Introduction

Planets with non-zero obliquity (tilted planets) will experience a seasonal cycle of the insolation meridional structure; during this seasonal cycle, the maximum insolation latitude shifts latitudinally from one hemisphere to the other, with the maximum latitude going poleward and the maximum insolation increasing with obliquity (Fig. 3). The obliquity seasonal cycle can be characterized by two periods during the orbital cycle, equinox, and solstice. Equinox is when the maximum insolation is at the equator; this occurs twice in a cycle, in this study at stellar longitudes 0° and 180° . Solstice is when the insolation peaks at the most poleward latitude, once at each hemisphere during the seasonal cycle; in this study, as a matter of convention, the southern hemisphere summer solstice (SHSS) is at stellar longitude

³ The potential temperature, $\theta = T(p_s/p)^\kappa$, where $\kappa = R_d/c_p$, is the temperature that an air parcel have had if it was brought adiabatically from some reference pressure (Hartmann 2016).

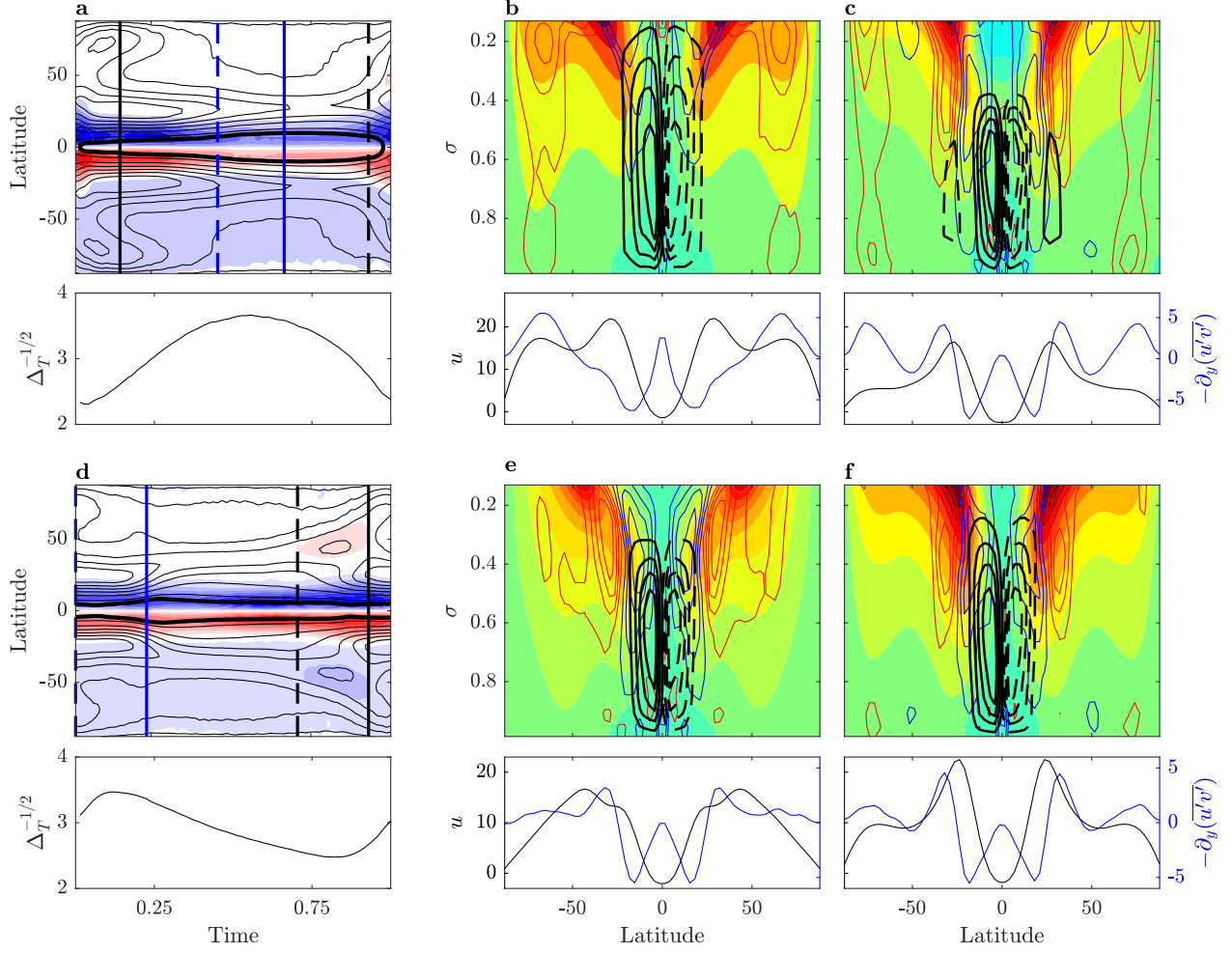


Figure 10. The seasonal cycle of the zonal mean zonal wind (\bar{u}) and mean meridional circulation (ψ). Panels a and d show the seasonal cycle of \bar{u} and ψ (top) and $\Delta_T^{-1/2}$ (bottom) for $\epsilon = 0.5$ and $\omega = 1$, and $\epsilon = 0.3$ and $\omega = 4$, respectively. Vertical lines represent the time average for panels b and e (black), and c and f (blue), with the dashed line representing the beginning of the average period. Panels b, c, e, and f, top shows the time mean of the zonal mean zonal wind (shading), mean meridional circulation (black contours, dashed lines are counter-clockwise circulation) and zonal mean eddy momentum flux convergence ($-\partial_y(u'v')$, red and blue contours, red is for convergence); bottom shows the vertically averaged \bar{u} (black) and $-\partial_y(u'v')$ (blue).

90° , and the summer hemisphere winter solstice (SHWS, alternatively the northern hemisphere summer solstice) is at stellar longitude 270° .

For a tilted planet in an elliptical orbit (non-zero eccentricity), the stellar longitude of perihelion (Π), e.g., the position where the planet is closest to its host star, relative to equinox is important. Note, that in this study, the stellar longitude of perihelion also denotes its phase with equinox (as equinox remains at stellar longitude 0°). Due to the importance of the perihelion position, it is essential to distinguish between different orbital configurations, that can be generally classified into four types: Alignment of perihelion with equinox ($\Pi = 0^\circ$, Fig. 11a) perihelion is after equinox and be-

fore the SHSS ($\Pi = 45^\circ$, Fig. 11b), perihelion aligned with SHSS ($\Pi = 90^\circ$, Fig. 11c) and perihelion after SHSS and before equinox ($\Pi = 135^\circ$, Fig. 11d). Note that perihelion values of $180^\circ - 315^\circ$ are a mirror image on the other hemisphere (assuming hemispheric symmetry). For a given obliquity and eccentricity values, different positions of perihelion will result in different insolation seasonal cycles depending on the different orbital parameters (Fig. 3g-i, 12e-h).

In an eccentric orbit, the orbital velocity is not constant during the orbital period, and depends on the planet's distance from the star, with faster orbital velocity as the planet comes closer to its host star (Lisauer & de Pater 2013). As eccentricity increases, this

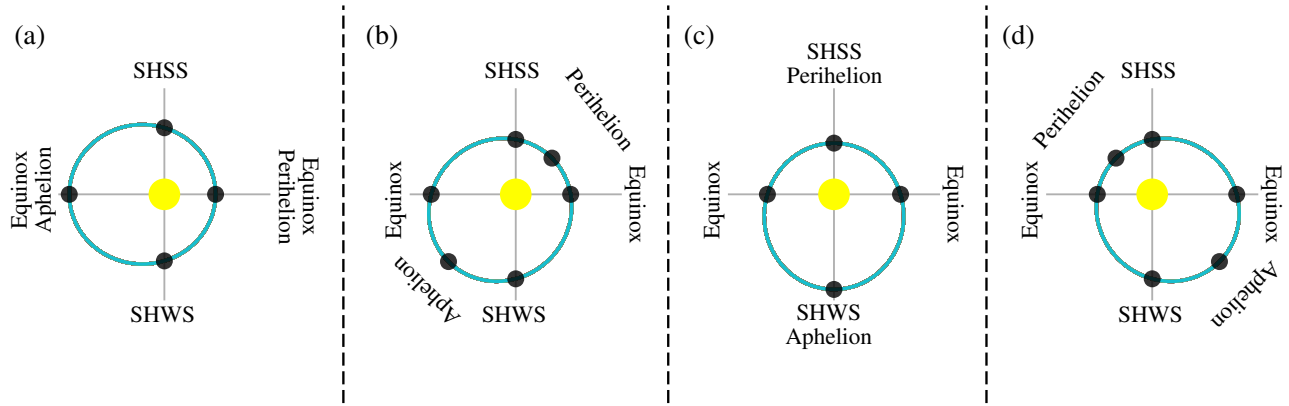


Figure 11. Distinctive orbital configurations for an orbit with non-zero obliquity and eccentricity. (a) Perihelion and equinox are aligned ($\Pi = 0^\circ$). (b) Perihelion after Equinox and before southern hemisphere summer solstice (SHSS, $\Pi = 45^\circ$). (c) Perihelion and SHSS are aligned ($\Pi = 180^\circ$). (d) Perihelion after southern hemisphere winter solstice (SHWS) and before Equinox ($\Pi = 135^\circ$).

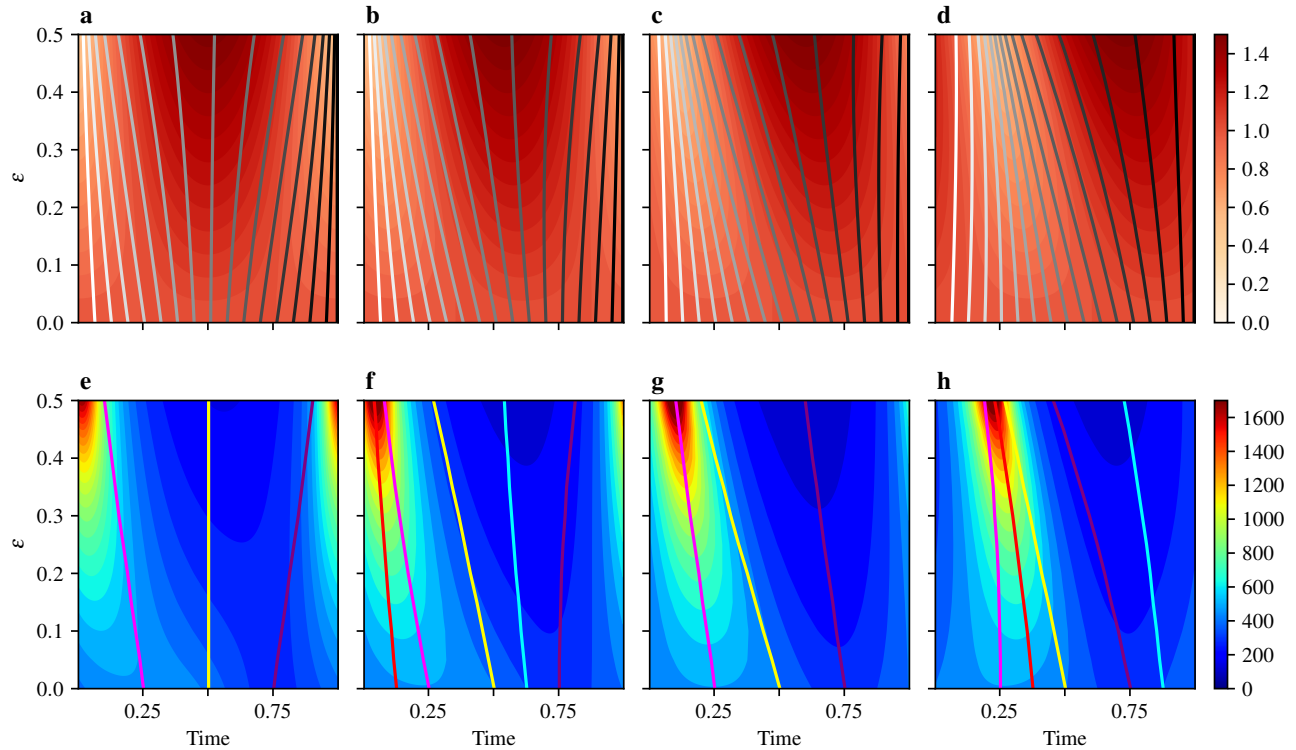


Figure 12. Top row: the normalized distance from the host star (shading) and the angle relative to equinox (contours, colors value are from 0° (white) to 359° (black)) as a function of eccentricity and time, for the four configurations showed in Figure 11, respectively. Bottom row: the insolation at latitude 23° in the southern hemisphere (shading), magenta line is for SHSS, yellow line is for second equinox (180°), purple line for SHWS, red line if for perihelion and cyan line is for aphelion. All plots are with obliquity 23° .

effect is magnified, and equal orbital distances will pass in a different timescales. This effect is illustrated in the first row of Figure 12, where, as the distance to the star becomes shorter (brighter colors), the contours, representing the orbital angle, become denser. This means

that changes in the insolation will occur over different timescales during the orbital period, depending on the orbital configuration (Figs. 3,12e-h), where, in general, as eccentricity increases, stronger forcing will occur over shorter periods (Fig. 12e-h).

To summarize, the combination of eccentricity and obliquity introduces a new degree of freedom, which is the relative position of the perihelion with respect to equinox. The complexity is emphasized by insolation changes occurring over different timescales, depending on the orbital configuration (Fig. 12). As a result, the study of the climate on a tilted planet in an eccentric orbit will depend on a wide range of parameters. The purpose of this section is to show preliminary results of the climate dependence on obliquity, eccentricity, and perihelion to serve as a baseline for future studies, give some constraints on the atmospheric circulation and discuss the importance and relevance of the different planetary parameters that can affect the climate response to changes in the orbital configuration.

4.2. Results

The insolation of a tilted planet with an eccentric orbit is a function of three parameters, obliquity (γ), eccentricity (ε), and perihelion (Π). This dependence implies that determining the climate on such a planet is a complex problem that depends on a large number of parameters. In order to examine the role of the different parameters, we conduct a series of simulations varying these three parameters. Of these three parameters, the most studied in the context of the atmospheric circulation, is the obliquity (e.g., Guendelman & Kaspi 2019; Lobo & Bordoni 2020; Ohno & Zhang 2019), these studies show the influence of the seasonal cycle on the climate and the importance of considering other parameters that relate to the atmospheric radiative timescale response when taking into account seasonal changes (Guendelman & Kaspi 2019). Increasing obliquity results in a stronger seasonal cycle of the insolation (Fig. 3d-f) that, in turn, results in a strong temperature and circulation seasonal cycle that increases with obliquity (Guendelman & Kaspi 2019; Lobo & Bordoni 2020).

A dominant feature of the surface temperature response is the time delay between the insolation and the temperature response. As mentioned, equinox is at stellar longitude 0° , also the first time step for all simulations, meaning that at the first time step, the insolation peaks at the equator. However, due to the atmospheric and surface radiative timescales (a slab ocean with a 10 m mixed layer), the temperature has a time lag with the radiative forcing. This time lag is not the same in all simulations and depends on eccentricity and perihelion (Figs. 13 and 14). This is a result of the dependence of the time period in which radiative changes occur during the seasonal cycle on eccentricity and perihelion, where close to perihelion, the changes are fast becoming faster with increasing eccentricity. In addition, close to perihe-

lion, there is usually a peak in the insolation (Fig. 12e-h), which increases with eccentricity, and as a response, the atmosphere will get warmer, resulting in a shorter radiative timescale (Eq. 7).

As a result of the eccentric orbit, there is an asymmetry between different hemispheres at similar seasons (for example, differences between summer at the northern hemisphere compared to summer at the southern hemisphere or differences between the two equinoxes). These differences will manifest in the seasons' mean temperature, meridional temperature gradient, and the length of each season. For example, for perihelion at equinox, an increase in eccentricity will result in one short and warm equinox, while the other equinox will be long and cold. The short equinox also means a fast transition between one solstice to the other, and as a result of the atmosphere and surface thermal inertia, a difference between the two solstice seasons duration and strength (Fig. 13), although the insolation is the same for both (Fig. 3g). In contrast to the seasonal cycle of a tilted planet in a circular orbit, where the seasonal maximum and minimum temperatures are at the same time (at opposite hemispheres, Guendelman & Kaspi 2019), in an eccentric orbit the seasonal maximum and minimum temperatures can be separated in time, with this separation increasing with eccentricity (Fig. 13). Note that this effect is strongly dependent on the perihelion position, where for perihelion at solstice, there is an alignment in time between the seasonal maximum and minimum temperatures (Fig. 14). In this case, the main effect of eccentricity is the asymmetry between the hemispheres, where one experiences an extreme winter and summer, while in the other hemisphere, the winter and summer are moderate.

The mean meridional circulation during the seasonal cycle is dominated mainly by a winter cell; meaning that during the majority of the year the circulation is composed of one cross-equatorial cell, with air rising in the summer hemisphere and descending in the winter hemisphere, and the transition seasons are relatively short (Figs. 13 and 14). Note that similar to the temperature response, there is also an asymmetry between the time periods of the circulation for each solstice season, where usually there is one season that is shorter where the circulation is generally stronger. The stronger circulation also occurs when the maximum temperature is at its most poleward position, and when it is closest to perihelion, e.g., warmer, and this period generally has also higher Δ_T values. This correlation between the strength of the circulation, Δ_T , and ϕ_0 is in agreement with axisymmetric arguments (Lindzen & Hou 1988; Guendelman & Kaspi 2018, 2019). Similar arguments are given

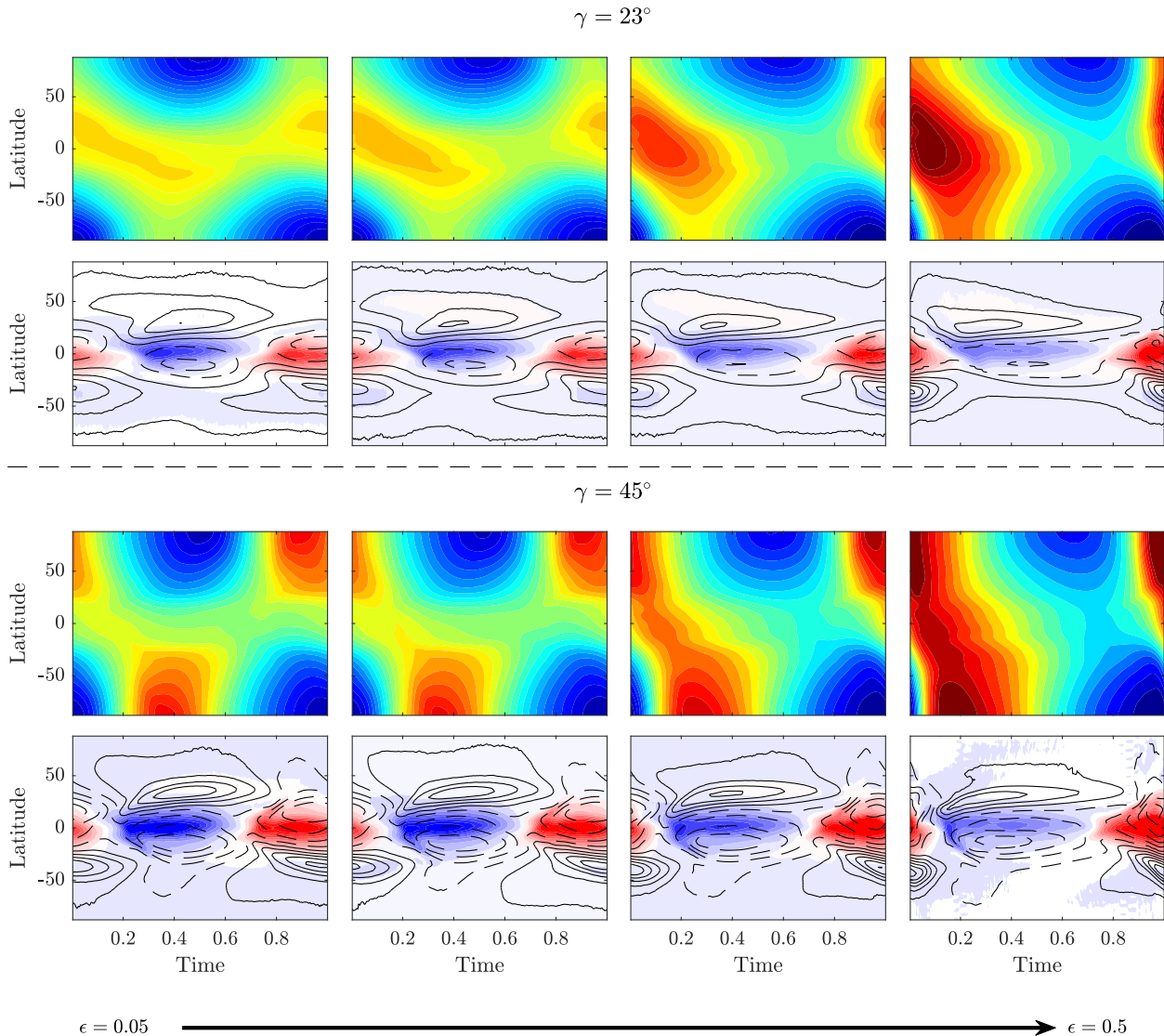


Figure 13. The seasonal cycle dependence on eccentricity for obliquity 23° (top half) and 45° (bottom half). Top row shows the seasonal cycle of the surface temperature colors ranging from 250° to 320° K. Bottom row shows the seasonal cycle of the mean meridional circulation, vertically averaged between 400 to 600 hPa (shading) and the zonal mean zonal wind vertically averaged between 100 to 500 hPa (blue means northward flow in the upper branch of the circulation). Eccentricity increases from left to right, with values of 0.05, 0.1, 0.3, 0.5.

for the width of the circulation, $Y_w = |\phi_a - \phi_d|$, where ϕ_a is the latitude of the ascending branch, and ϕ_d is the latitude of the descending branch (both in radians), Y_w is the width of the Hadley cell. According to the axisymmetric theory, as ϕ_0 goes more poleward, and larger Δ_T corresponds to wider circulation (Guendelman & Kaspi 2018). That being said, there is a constraint on the circulation width (more specifically the ascending branch of the circulation) that rises from axisymmetric considerations (Guendelman & Kaspi 2018; Hill et al. 2019; Singh 2019), where for planets with low thermal Rossby number R_o (Eq. 23) the ascending branch will remain

at midlatitudes, even if the maximum temperature is at the pole (Guendelman & Kaspi 2018). Although these arguments are derived for a perpetual solstice case, and thus assuming fast adjustment to the radiative forcing, an assumption that is not necessarily accurate for this case, there is still a clear correlation between Y_w and R_o , that becomes clearer (less spread) if we take into account also the effect of ϕ_0 (Fig. 15). The spread of the Y_w in Figure 15 can be a result of several reasons: first, this is not a perpetual case, meaning that the seasonal cycle is important. Second, to calculate R_o , we parameterize the different parameters (Δ_T , H) using the model

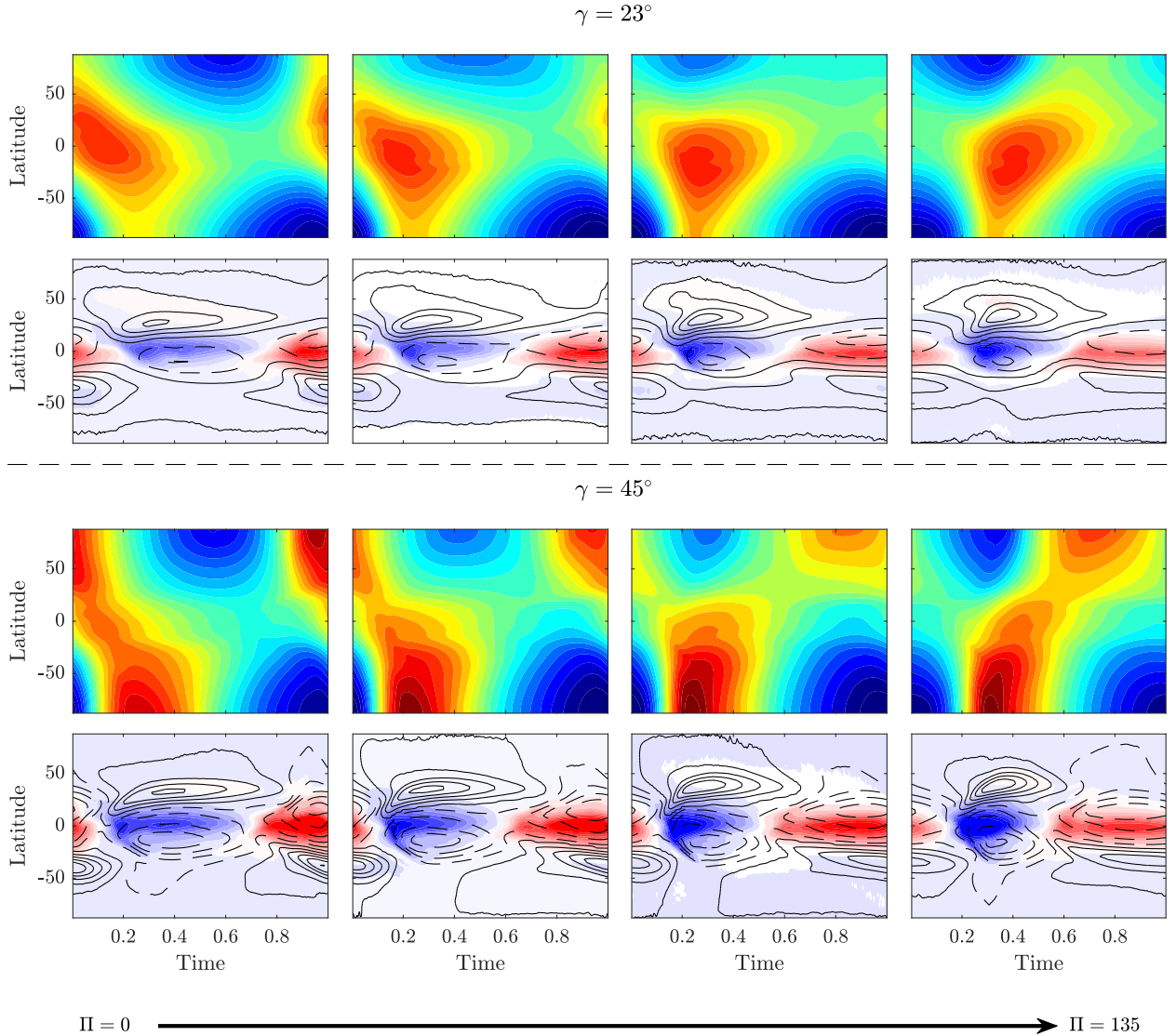


Figure 14. Similar to Figure 13, for perihelion. Perihelion increases from left to right, with values of 0, 45, 90, 135.

output, although, in the original theory, these parameters are input parameters of the model (Lindzen & Hou 1988).

Although the temperature response seems to follow the seasonal solar forcing, there is a need to examine the details of the seasonal cycle response. For example, looking at the cell width dependence on R_o , there seems to be a transition in the scaling between a linear response to a more complex power law (Fig. 15). The axisymmetric prediction is that the width of the circulation will follow $R_o^{1/2}$ for perpetual equinox (Held & Hou 1980), and $R_o^{1/3}$ for the perpetual solstice case (Caballero et al. 2008). Following that, we can assume that the different scaling in Figure 15 can be a result of the seasonal cycle transition from a perpetual equinox scaling to perpet-

ual solstice during the seasonal cycle. Alternatively, it is possible that this regime transition is not a transition within the axisymmetric scaling, but rather transition from eddy mediated equinox circulation to an axisymmetric solstice circulation similar to the transition suggested by Bordoni & Schneider (2010). A differentiation between the two can help explain the mechanism of the response of the subtropical jet, where generally, the jet is stronger when the circulation is stronger and wider.

4.3. Discussion

Determining the climate on a tilted planet in an eccentric orbit is a complex problem that depends on various parameters. In addition to the dependence on the orbital parameters γ , ε , Π , the climate will strongly depend on parameters that control the atmo-

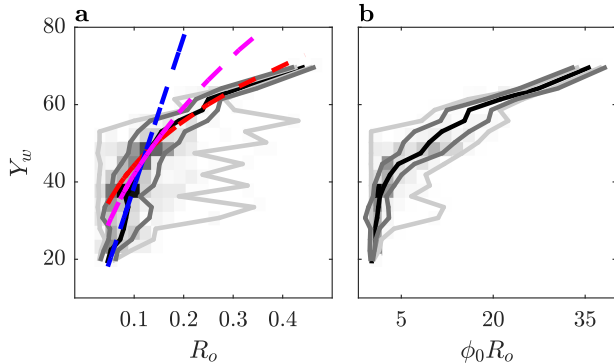


Figure 15. Hadley cell width (in latitude degrees) as a function of thermal Rossby number, R_o (a), and the product of the thermal Rossby number with the latitude of maximum surface temperature, $\phi_0 R_o$ (b) during the seasonal cycle of all the simulations (colors are occurrences, darker colors are for more abundant occurrence). Black line represents the bin average of the Y_w , dark gray lines are the standard deviations and the light gray lines are for all the points. Blue magenta and red line in (a) are lines with scaling of R_o , $R_o^{1/2}$ and $R_o^{1/3}$, respectively.

spheric response, mainly ones that relate to the radiative timescale. The orbital period, atmospheric mass, and surface heat capacity are an example of important parameters that will influence the resulting climate. Due to the variation in the timescales of the radiative changes during an eccentric orbit, the radiative timescale can significantly alter the climate response. The importance of the radiative timescale is also illustrated in section 3, where there is a qualitative difference in the climate response between short and long orbital. Examining the dependence of the climate response also on the radiative timescale or orbital period can also help to illuminate between in the detailed seasonal cycle response.

In contrast to the zero obliquity case, where the perpetual equinox dependence on the solar constant can be considered as the extreme limit of an infinitely long orbital period, there is no simple analog study for the non-zero obliquity case. The analog study in the non-zero obliquity case will be performing a perpetual study for each day in the seasonal cycle, and for each day, study its sensitivity to solar constant variations. Even if one does this type of study, its relevance will be for very long orbital periods, as the timescale changes during the insolation seasonal cycle play an important role, and its importance increases with increasing eccentricity. Nonetheless, this type of study can act as a limit to compare with the seasonal cycle response and can help to differentiate the seasonal transient effects.

5. CONCLUSIONS

Studying the possible climate of exoplanets obliges us to think about the different possible orbital configurations and their effects on the climate. The simpler configurations are those where the insolation is time independent, for example, perpetual equinox (Kaspi & Showman 2015), tidally locked (Merlis & Schneider 2010), and perpetual reverse climates (Kang et al. 2019). However, it is probable that a large number, if not the majority of the planets, will experience significant temporal variation in solar insolation, where the perpetual case is no longer relevant. In this study, we focus on the effect of eccentricity on the diurnal mean climate for planets with zero and non-zero obliquity. It is important to note that changes in eccentricity and obliquity are not only between different planets but also during different time periods of a single planet that experiences Milankovich-like cycles (Spiegel et al. 2010; Way & Georganakarakos 2017), rendering this question even more relevant.

The insolation variations for a planet with zero obliquity in an eccentric orbit are equivalent to changes of the solar constant during the seasonal cycle. For this reason, studying the perpetual equinox response to variations in the solar constant is a good baseline for comparison with the seasonal cycle. Increasing the solar constant results in a trivial increase in temperature, however, the resulting climate can differ significantly between planets, depending on the moisture content of the atmosphere (Fig. 4). In the moist case, due to the non-linearity of water vapor with temperature, the heat transport becomes more efficient (due to latent heat flux, Fig. 5), resulting in a decrease of Δ_T with S_0 , opposite to the dry case (Fig. 4a). These differences in the response have a strong effect on the atmospheric temperature profile, and alter the dynamical response between moist and dry cases, emphasizing the role of moisture. This moisture-like dependence works for water, but in general, for any atmosphere with a condensible element, for example, methane on Titan (Mitchell et al. 2009; Newman et al. 2016).

When including seasonal variations, the radiative variations timescales and the atmospheric response becomes important, and the resulting climate will strongly depend on the ratio between the radiative timescale and the orbital period. For very short orbital periods, the main response of the atmosphere is to the annual mean forcing, where there is an increase in the mean flux with ε (Bolmont et al. 2016) (Fig. 6c, e). As the orbital period becomes longer there is a transition, where, in short to moderate orbital periods the response is dominated by a simple energy balance, In long orbital periods, other processes come into play, resulting in a more similar re-

response to the perpetual case to changes in S_0 (Figs. 6, 8). The response of the atmosphere to eccentricity changes in a zero obliquity planet is sensitive to the radiative changes timescale and the radiative timescale of the atmosphere, and more specifically, to the latitudinal structure of the radiative timescale (Fig. 8). The dynamics also undergoes a seasonal cycle, where, due to the seasonal changes in Δ_T the mean meridional circulation changes in strength and height during the seasonal cycle and the number of eddy driven jets change during the seasonal cycle, due to changes in eddy character and the resulting Rhines scale (Fig. 10).

Combining changes in obliquity and eccentricity becomes more complex as in addition to these two parameters the relative position between equinox and perihelion can result in different insolation patterns (Fig. 3), making the solar forcing dependent on these three parameters (Fig. 12). As part of the insolation changes, the timescale of these changes also depends on the orbital configurations, meaning that during the seasonal cycle, the insolation changes that occur close to perihelion will have a short timescale whereas close to aphelion the changes will be on a longer timescale. These timescale differences will extenuate with increasing eccentricity. As a result, the seasonal cycle of a tilted planet in an eccentric orbit is complex, with similar seasons having different climate at each hemisphere. Also, different seasons will have different timescales, for example, in the case of perihelion at equinox, there will be a fast transition between the two solstice seasons (Figs. 13, 14).

These fast transitions in the temperature result in the circulation also experiencing fast transitions during the seasonal cycle. During the seasonal cycle, most of the time, the Hadley circulation is composed of one cross-equatorial cell with air rising off the equator (with its

direction depending on the specific season), with relative short transition periods of two cells with air rising close to the equator. As in the temperature response, the period of each season is different, where usually the short season (close to perihelion) has a stronger and wider circulation. A good constraint on the circulation response is the thermal Rossby number, and latitude of maximum temperature, where poleward ϕ_0 and higher R_o will generally mean a stronger and wider circulation (Figs. 13-15).

Although the general response seems to follow the insolation, which puts a strong constraint on the circulation response, the details of the seasonal cycle can be complex (Merlis et al. 2013). A more detailed examination of the seasonal cycle in all the different orbital configuration is needed in order to better understand the climate on tilted planets in an eccentric orbit. Also, it is possible that similar to the zero obliquity case, if considering parameters such as the orbital period and ones that relate to the surface and atmosphere radiative timescale, there will be a qualitative difference in the atmospheric response.

In this study, we have shown the complexity of the seasonal response to variations in the orbital configuration. This complexity emphasizes the importance of understanding the seasonal cycle, as in the presence of a seasonal cycle, the climate differs substantially from the perpetual climate or the annual mean climate. It is reasonable to assume that many of the observed exoplanets have a wide variety of orbital configurations. These new and future understandings of the climate dependence on orbital configuration will help to advance the understanding of climate dynamics and might inspire future exoplanetary observations, as for the early theory superrotation in hot-Jupiters (Showman, A. P. & Guillot, T. 2002; Knutson et al. 2007).

REFERENCES

- Adams, A. D., Boos, W. R., & Wolf, E. T. 2019, *AJ*, 157, 189, doi: [10.3847/1538-3881/ab107f](https://doi.org/10.3847/1538-3881/ab107f)
- Andrews, D. G. 2010, *An Introduction to Atmospheric Physics*, 2nd edn. (Cambridge University Press), doi: [10.1017/CBO9780511800788](https://doi.org/10.1017/CBO9780511800788)
- Bolmont, E., Libert, A.-S., Leconte, J., & Selsis, F. 2016, *A&A*, 591, A106, doi: [10.1051/0004-6361/201628073](https://doi.org/10.1051/0004-6361/201628073)
- Bordoni, S., & Schneider, T. 2010, *JAtS*, 67, 1643, doi: [10.1175/2009JAS3294.1](https://doi.org/10.1175/2009JAS3294.1)
- Caballero, R., Pierrehumbert, R. T., & Mitchell, J. L. 2008, *QJRM*, 134, 1269, doi: [10.1002/qj.271](https://doi.org/10.1002/qj.271)
- Chemke, R., & Kaspi, Y. 2015a, *JAtS*, 72, 3891, doi: [10.1175/JAS-D-15-0007.1](https://doi.org/10.1175/JAS-D-15-0007.1)
- . 2015b, *JAMES*, 7, 1457, doi: [10.1002/2015MS000481](https://doi.org/10.1002/2015MS000481)
- . 2017, *ApJ*, 845, 1, doi: [10.3847/1538-4357/aa7742](https://doi.org/10.3847/1538-4357/aa7742)
- Dressing, C. D., Spiegel, D. S., Scharf, C. A., Menou, K., & Raymond, S. N. 2010, *ApJ*, 721, 1295, doi: [10.1088/0004-637X/721/2/1295](https://doi.org/10.1088/0004-637X/721/2/1295)
- Frierson, D. M. W., Held, I. M., & Zurita-Gotor, P. 2006, *JAtS*, 63, 2548, doi: [10.1175/JAS3753.1](https://doi.org/10.1175/JAS3753.1)
- Galanti, E., Kaspi, Y., & Tziperman, E. 2017, *JFM*, 810, 175195, doi: [10.1017/jfm.2016.687](https://doi.org/10.1017/jfm.2016.687)
- Gilliland, R. L., Marcy, G. W., Rowe, J. F., et al. 2013, *ApJ*, 766, 40, doi: [10.1088/0004-637X/766/1/40](https://doi.org/10.1088/0004-637X/766/1/40)
- Guendelman, I., & Kaspi, Y. 2018, *Geophys. Res. Lett.*, 45, 13, doi: [10.1029/2018GL080752](https://doi.org/10.1029/2018GL080752)

- . 2019, *ApJ*, 881, 67, doi: [10.3847/1538-4357/ab2a06](https://doi.org/10.3847/1538-4357/ab2a06)
- Hartmann, D. L. 2016, *Global Physical Climatology* (Second Edition), second edition edn. (Boston: Elsevier), doi: <https://doi.org/10.1016/B978-0-12-328531-7.00019-0>
- Held, I. M., & Hou, A. Y. 1980, *JAtS*, 37, 515, doi: [10.1175/1520-0469\(1980\)037<0515:NASCIA>2.0.CO;2](https://doi.org/10.1175/1520-0469(1980)037<0515:NASCIA>2.0.CO;2)
- Hill, S. A., Bordini, S., & Mitchell, J. L. 2019, *JAtS*, 76, 1547, doi: [10.1175/JAS-D-18-0306.1](https://doi.org/10.1175/JAS-D-18-0306.1)
- Howard, A. W. 2013, *Sci*, 340, 572, doi: [10.1126/science.1233545](https://doi.org/10.1126/science.1233545)
- Hut, P. 1981, *A&A*, 99, 126, <http://adsabs.harvard.edu/abs/1981A%26A....99..126H>
- Ingersoll, A. P. 1990, *Sci*, 248, 308, doi: [10.1126/science.248.4953.308](https://doi.org/10.1126/science.248.4953.308)
- Kane, S. R., & Torres, S. M. 2017, *AJ*, 154, 204, doi: [10.3847/1538-3881/aa8fce](https://doi.org/10.3847/1538-3881/aa8fce)
- Kang, W., Cai, M., & Tziperman, E. 2019, *Icar*, 330, 142, doi: <https://doi.org/10.1016/j.icarus.2019.04.028>
- Kaspi, Y., & Showman, A. P. 2015, *ApJ*, 804, 60, doi: [10.1088/0004-637X/804/1/60](https://doi.org/10.1088/0004-637X/804/1/60)
- Kataria, T., Showman, A. P., Lewis, N. K., et al. 2013, *ApJ*, 767, 76, doi: [10.1088/0004-637X/767/1/76](https://doi.org/10.1088/0004-637X/767/1/76)
- Knutson, H. A., Charbonneau, D., Allen, L. E., et al. 2007, *Natur*, 447, 183, doi: [10.1038/nature05782](https://doi.org/10.1038/nature05782)
- Komacek, T. D., & Abbot, D. S. 2019, *ApJ*, 871, 245, doi: [10.3847/1538-4357/aafb33](https://doi.org/10.3847/1538-4357/aafb33)
- Kopparapu, R. K., Ramirez, R., Kasting, J. F., et al. 2013, *ApJ*, 765, 131, doi: [10.1088/0004-637X/765/2/131](https://doi.org/10.1088/0004-637X/765/2/131)
- Lachmy, O., & Harnik, N. 2014, *JAtS*, 71, 1389, doi: [10.1175/JAS-D-13-0125.1](https://doi.org/10.1175/JAS-D-13-0125.1)
- Laraia, A. L., & Schneider, T. 2015, *JAtS*, 72, 4281, doi: [10.1175/JAS-D-15-0030.1](https://doi.org/10.1175/JAS-D-15-0030.1)
- Lee, S. 2005, *JAtS*, 62, 2484, doi: [10.1175/JAS3481.1](https://doi.org/10.1175/JAS3481.1)
- Levine, X. J., & Schneider, T. 2015, *JAtS*, 72, 2744, doi: [10.1175/JAS-D-14-0152.1](https://doi.org/10.1175/JAS-D-14-0152.1)
- Lewis, N. K., Parmentier, V., Kataria, T., et al. 2017, arXiv:1706.00466 [astro-ph], <http://arxiv.org/abs/1706.00466>
- Lewis, N. K., Showman, A. P., Fortney, J. J., Knutson, H. A., & Marley, M. S. 2014, *ApJ*, 795, 150, doi: [10.1088/0004-637X/795/2/150](https://doi.org/10.1088/0004-637X/795/2/150)
- Lewis, N. K., Showman, A. P., Fortney, J. J., et al. 2010, *ApJ*, 720, 344, doi: [10.1088/0004-637X/720/1/344](https://doi.org/10.1088/0004-637X/720/1/344)
- Lindzen, R. S., & Hou, A. V. 1988, *JAtS*, 45, 2416, doi: [10.1175/1520-0469\(1988\)045<2416:HCFZAH>2.0.CO;2](https://doi.org/10.1175/1520-0469(1988)045<2416:HCFZAH>2.0.CO;2)
- Linsenmeier, M., Pascale, S., & Lucarini, V. 2015, *Planet. Space Sci.*, 105, 43, doi: [10.1016/j.pss.2014.11.003](https://doi.org/10.1016/j.pss.2014.11.003)
- Lissauer, J. J., & de Pater, I. 2013, *Fundamental Planetary Science: Physics, Chemistry and Habitability* (Cambridge University Press), doi: [10.1017/CBO9781139050463](https://doi.org/10.1017/CBO9781139050463)
- Lobo, A. H., & Bordini, S. 2020, *Icar*, 340, 113592, doi: <https://doi.org/10.1016/j.icarus.2019.113592>
- Merlis, T. M., & Schneider, T. 2010, *JAMES*, 2, doi: [10.3894/JAMES.2010.2.13](https://doi.org/10.3894/JAMES.2010.2.13)
- Merlis, T. M., Schneider, T., Bordini, S., & Eisenman, I. 2013, *JCLI*, 26, 740, doi: [10.1175/JCLI-D-11-00716.1](https://doi.org/10.1175/JCLI-D-11-00716.1)
- Mitchell, J. L., Pierrehumbert, R. T., Frierson, D. M., & Caballero, R. 2009, *Icar*, 203, 250, doi: <https://doi.org/10.1016/j.icarus.2009.03.043>
- Mitchell, J. L., & Vallis, G. K. 2010, *JGRE*, 115, doi: [10.1029/2010JE003587](https://doi.org/10.1029/2010JE003587)
- Mndez, A., & Rivera-Valentn, E. G. 2017, *ApJ*, 837, L1, doi: [10.3847/2041-8213/aa5f13](https://doi.org/10.3847/2041-8213/aa5f13)
- Newman, C. E., Richardson, M. I., Lian, Y., & Lee, C. 2016, *Icar*, 267, 106, doi: <https://doi.org/10.1016/j.icarus.2015.11.028>
- Ohno, K., & Zhang, X. 2019, *ApJ*, 874, 1, doi: [10.3847/1538-4357/ab06cc](https://doi.org/10.3847/1538-4357/ab06cc)
- Polichtchouk, I., & Cho, J. Y.-K. 2016, *QJRMS*, 142, 1528, doi: [10.1002/qj.2755](https://doi.org/10.1002/qj.2755)
- Rhines, P. B. 1975, *JFM*, 69, 417443, doi: [10.1017/S0022112075001504](https://doi.org/10.1017/S0022112075001504)
- . 1979, *AnRFM*, 11, 401, doi: [10.1146/annurev.fl.11.010179.002153](https://doi.org/10.1146/annurev.fl.11.010179.002153)
- Rose, B. E., Cronin, T. W., & Bitz, C. M. 2017, *ApJ*, 846, 28, doi: [10.3847/1538-4357/aa8306](https://doi.org/10.3847/1538-4357/aa8306)
- Showman, A. P., & Guillot, T. 2002, *A&A*, 385, 166, doi: [10.1051/0004-6361:20020101](https://doi.org/10.1051/0004-6361:20020101)
- Singh, M. S. 2019, *JAtS*, 76, 1989, doi: [10.1175/JAS-D-18-0341.1](https://doi.org/10.1175/JAS-D-18-0341.1)
- Spiegel, D. S., Raymond, S. N., Dressing, C. D., Scharf, C. A., & Mitchell, J. L. 2010, *ApJ*, 721, 1308, doi: [10.1088/0004-637X/721/2/1308](https://doi.org/10.1088/0004-637X/721/2/1308)
- Vallis, G. K. 2017, *Atmospheric and Oceanic Fluid Dynamics: Fundamentals and Large-Scale Circulation*, 2nd edn. (Cambridge University Press), doi: [10.1017/9781107588417](https://doi.org/10.1017/9781107588417)
- Vallis, G. K., Zurita-Gotor, P., Cairns, C., & Kidston, J. 2015, *QJRMS*, 141, 1479, doi: [10.1002/qj.2456](https://doi.org/10.1002/qj.2456)
- Wang, Y., Read, P. L., Tabataba-Vakili, F., & Young, R. M. B. 2018, *QJRMS*, 144, 2537, doi: [10.1002/qj.3350](https://doi.org/10.1002/qj.3350)
- Wang, Y., Tian, F., & Hu, Y. 2014, *ApJ*, 791, L12, doi: [10.1088/2041-8205/791/1/L12](https://doi.org/10.1088/2041-8205/791/1/L12)
- Way, M. J., & Georgakarakos, N. 2017, *ApJ*, 835, L1, doi: [10.3847/2041-8213/835/1/L1](https://doi.org/10.3847/2041-8213/835/1/L1)
- Williams, D. M., & Pollard, D. 2002, *IJAsB*, 1, 61, doi: [10.1017/S1473550402001064](https://doi.org/10.1017/S1473550402001064)

- Wolf, E. T., Shields, A. L., Kopparapu, R. K., Haqq-Misra, J., & Toon, O. B. 2017, *ApJ*, 837, 107,
doi: [10.3847/1538-4357/aa5ffc](https://doi.org/10.3847/1538-4357/aa5ffc)
- Yuval, J., & Kaspi, Y. 2018, *JAtS*, 75, 1371,
doi: [10.1175/JAS-D-17-0139.1](https://doi.org/10.1175/JAS-D-17-0139.1)